

Path integral molecular dynamics for thermodynamics and Green's function of ultracold spinor bosons

Yongle Yu,¹ Shujuan Liu,² Hongwei Xiong,² and Yunuo Xiong^{2, a)}

¹*Innovation Academy for Precision Measurement Science and Technology, Chinese Academy of Sciences, Wuhan 430071, P. R. China*

²*College of Science, Zhejiang University of Technology, Hangzhou 31023, P. R. China*

Most recently, the path integral molecular dynamics has been successfully used to consider the thermodynamics of single-component identical bosons and fermions. In this work, the path integral molecular dynamics is developed to simulate the thermodynamics, Green's function and momentum distribution of two-component bosons in three dimensions. As an example of our general method, we consider the thermodynamics of up to sixteen bosons in a three-dimensional harmonic trap. For noninteracting spinor bosons, our simulation shows a bump in the heat capacity. As the repulsive interaction strength increases, however, we find the gradual disappearance of the bump in the heat capacity. We believe this simulation result can be tested by ultracold spinor bosons with optical lattices and magnetic-field Feshbach resonance to tune the inter-particle interaction. We also calculate Green's function and momentum distribution of spinor bosons. Our work facilitates the exact numerical simulation of spinor bosons, whose property is one of the major problems in ultracold Bose gases.

^{a)}Electronic mail: 2111909023@zjut.edu.cn

I. INTRODUCTION

The exact numerical simulation of identical particles at finite temperature or zero temperature is one of the major problems in quantum physics. The so-called exact numerical simulation means that we should not assume in advance the trial wave function¹ or assume the usual contact interaction^{2,3} for the convenience of calculations. The exact numerical simulation of the thermodynamics of identical particles requests that we carry out the theoretical studies directly from the partition function of the quantum system. Fortunately, without predetermining any properties of the quantum system, the partition function in the path integral formalism⁴⁻⁶ can be mapped to an equivalent classical ensemble of interacting ring polymers⁷⁻²⁸. However, during this mapping, one of the key obstacles we face is how to give exact consideration of quantum exchange effects for identical particles. In a pioneering work²⁹ on single-component identical bosons, a recursion formula is found to express the partition function in a highly efficient way. In Ref.³⁰, path integral molecular dynamics (PIMD) and the recursion formula are generalized to calculate Green's function and momentum distribution of single-component bosons. Other recent advances include the application of PIMD to supersolid phase in high-pressure deuterium³¹ and bosons in singular magnetic field³², and the generalization of PIMD to spin-polarized fermions³³⁻³⁵. In particular, PIMD was used most recently to consider the fermion sign problem for large fermion system³⁵.

Of course, we need to generalize PIMD to two-component (or spinor) bosons, because this is very common in quantum gases, in particular with intensive experimental and theoretical studies on ultracold spinor bosons³⁶⁻⁴⁰. The purpose of the present work is to develop PIMD for two-component bosons with the same intracomponent and intercomponent interaction, and it is straightforward to generalize our method to different intracomponent and intercomponent interactions. Different from previous PIMD simulation^{29,30,32-35} for identical particles in two dimensions, here we consider spinor bosons in three dimensions and study the number of beads (in PIMD simulation) needed in numerical simulation to achieve numerical convergence. As an example, we consider the thermodynamics of two-component bosons in a three-dimensional harmonic trap. The energy and heat capacity are calculated to show the role of temperature and repulsive interaction in the thermodynamics of ultracold spinor bosons. We also generalize previous method^{30,34} to calculate Green's function and momentum distribution of spinor bosons to pave the way of the general application of PIMD

for ultracold spinor Bose gases.

II. THE PARTITION FUNCTION FOR TWO-COMPONENT SPINOR BOSONS

We consider in this work spinor bosons with two internal states denoted by $|\uparrow\rangle$ and $|\downarrow\rangle$. It is straightforward to generalize to more general M-component spinor bosons. We consider the following Hamiltonian operator which will not change the internal state of a boson:

$$\hat{H} = \sum_{j=1}^{N_{\uparrow}} \frac{\hat{\mathbf{p}}_j^2}{2m} + \sum_{j'=1}^{N_{\downarrow}} \frac{\hat{\mathbf{p}}_{j'}^2}{2m} + V(\hat{\mathbf{r}}_1, \dots, \hat{\mathbf{r}}_N). \quad (1)$$

Here N_{\uparrow} and N_{\downarrow} denote the particle numbers in the internal states $|\uparrow\rangle$ and $|\downarrow\rangle$, respectively. $N = N_{\uparrow} + N_{\downarrow}$ is the total particle number of the quantum system. Here V includes both the external potential and inter-particle interaction.

At finite temperature $\beta = 1/k_B T$, the partition function is

$$Z_B = \text{Tr} \left(e^{-\beta \hat{H}} \right). \quad (2)$$

The purpose of the present work is to develop the PIMD to calculate the thermodynamics of spinor bosons based on this partition function.

For two-component spinor bosons, we define the following basis which is invariant about the exchange of any two bosons:

$$|N_B\rangle \sim \sum_{p \in S_N} |p \{ \mathbf{r}_1^{\uparrow}, \dots, \mathbf{r}_{N_{\uparrow}}^{\uparrow}; \mathbf{r}_{N_{\uparrow}+1}^{\downarrow}, \dots, \mathbf{r}_N^{\downarrow} \} \rangle. \quad (3)$$

Here p represents $N!$ permutation operations on the index $\{1, 2, \dots, N_{\uparrow}, N_{\uparrow} + 1, \dots, N\}$. We do not change the order of the index for the internal state in the permutation summation.

In this case, the partition function Z_B for bosons is

$$Z_B \sim \int \prod_{j=1}^N d\mathbf{x}_j \langle N_B | e^{-\Delta\beta \hat{H}} \dots e^{-\Delta\beta \hat{H}} | N_B \rangle. \quad (4)$$

Here $\Delta\beta = \beta/P$ and P is the number of beads in PIMD. One of the difficulties to calculate the partition function is the $N! \times N!$ summation in the above expression.

Assume

$$|N\rangle = \left| \mathbf{r}_1^{\uparrow}, \dots, \mathbf{r}_{N_{\uparrow}}^{\uparrow}; \mathbf{r}_{N_{\uparrow}+1}^{\downarrow}, \dots, \mathbf{r}_N^{\downarrow} \right\rangle \quad (5)$$

without permutation summation, we have

$$Z_B \sim \int \prod_{j=1}^N d\mathbf{r}_j \langle N | e^{-\Delta\beta\hat{H}} \dots e^{-\Delta\beta\hat{H}} | N_B \rangle. \quad (6)$$

Now we consider the following identity operator

$$\hat{I}_B \sim \int \prod_{j=1}^N d\mathbf{r}_j | N_B \rangle \langle N_B|. \quad (7)$$

By inserting a series of this identity operator in Eq. (6), the partition function becomes:

$$Z_B \sim \int \prod_{j=1}^N d\mathbf{r}_j \langle N | e^{-\Delta\beta\hat{H}} \hat{I}_B e^{-\Delta\beta\hat{H}} \dots e^{-\Delta\beta\hat{H}} \hat{I}_B e^{-\Delta\beta\hat{H}} \hat{I}_B | N_B \rangle. \quad (8)$$

Without considering the exchange symmetry, we also have another form of the identity operator

$$\hat{I} = \int \prod_{j=1}^N d\mathbf{r}_j | N \rangle \langle N|. \quad (9)$$

In this case, it is easy to prove that

$$e^{-\beta\hat{H}} \hat{I}_B = e^{-\frac{\beta}{P}\hat{H}} \hat{I} e^{-\frac{\beta}{P}\hat{H}} \hat{I} \dots \hat{I} e^{-\frac{\beta}{P}\hat{H}} \hat{I}_B. \quad (10)$$

We get

$$Z_B \sim \int \prod_{j=1}^N d\mathbf{r}_j \langle N | e^{-\Delta\beta\hat{H}} \hat{I} e^{-\Delta\beta\hat{H}} \hat{I} \dots \hat{I} e^{-\Delta\beta\hat{H}} \hat{I} e^{-\Delta\beta\hat{H}} | N_B \rangle. \quad (11)$$

We see that for Hamiltonian operator which does not change the internal state of the bosons, in calculating the partition function, we should consider all the permutations due to the exchange symmetry for bosons in the same internal state. In Fig. 1, we illustrate an example of 3 bosons in internal state $|\uparrow\rangle$ and 3 bosons in internal state $|\downarrow\rangle$. The dashed line in this figure illustrates the interaction between particles, while the solid line shows the connection of the beads for the same particle. It is worthy to point out that in the integral $\int \prod_{j=1}^N d\mathbf{r}_j$, the coordinates are the same for $|N\rangle$ and $|N_B\rangle$. Hence, the permutation summation in $|N_B\rangle$ and closed ring polymer should be considered simultaneously.

There are $N_\uparrow! \times N_\downarrow!$ permutation summations for the partition function shown in Fig. 1, which increases exponentially with N . Fortunately, in a recent pioneering work²⁹, Hirshberg, Rizzi and Parrinello found that the partition function corresponding to a system of identical bosons without internal freedom can be calculated by a recursion formula which can be evaluated in $O(PN^3)$ time, providing an exponential speedup over simply summing all configurations for different permutations.

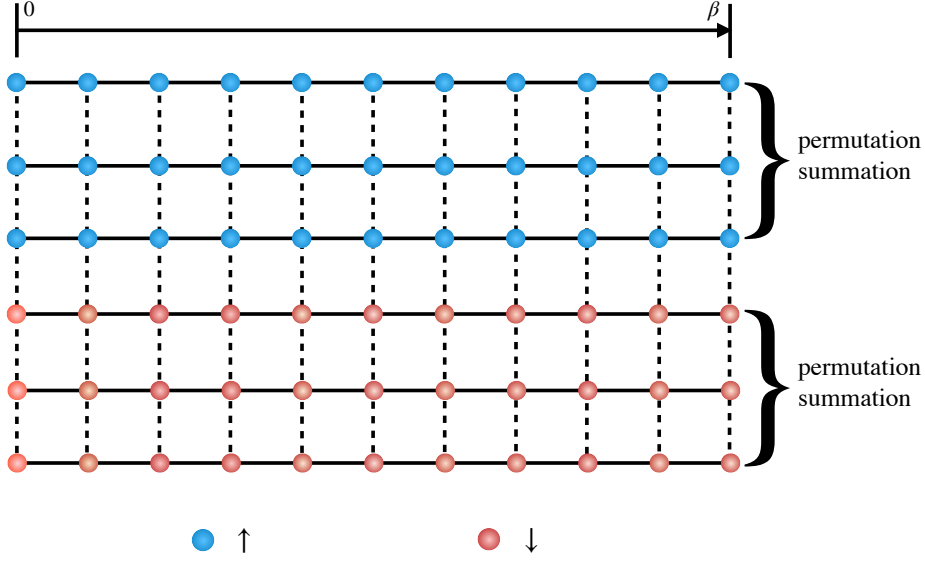


FIG. 1. Illustration of the ring polymers for the partition function of spinor bosons with two internal states $|\uparrow\rangle$ and $|\downarrow\rangle$. The solid line shows the connection of the beads for the same particle, while the dashed line shows the inter-particle interaction between particles at the same imaginary time.

Generalizing the recursion formula for single-component bosons, we get the following expression of the partition function for two-component bosons

$$Z_B = \left(\frac{mP}{2\pi\hbar^2\beta} \right)^{PdN/2} \int d\mathbf{R}_1 \dots d\mathbf{R}_N e^{-\beta U_B^{(N)}}. \quad (12)$$

The system under consideration has d spatial dimensions. Here \mathbf{R}_i represents the collection of ring polymer coordinates $(\mathbf{r}_i^1, \dots, \mathbf{r}_i^P)$ corresponding to the i th particle. In addition,

$$U_B^{(N)} = -\frac{1}{\beta} \ln W_B^{(N_\uparrow)} - \frac{1}{\beta} \ln W_B^{(N_\downarrow)} + \frac{1}{P} \sum_{j=1}^P V(\mathbf{r}_1^j, \dots, \mathbf{r}_N^j). \quad (13)$$

$$W_B^{(N_\uparrow)} = \frac{1}{N_\uparrow} \sum_{k=1}^{N_\uparrow} e^{-\beta E_{N_\uparrow}^{(k)}} W_B^{(N_\uparrow - k)}. \quad (14)$$

$$E_{N_\uparrow}^{(k)} = \frac{1}{2} m \omega_P^2 \sum_{l=N_\uparrow - k + 1}^{N_\uparrow} \sum_{j=1}^P (\mathbf{r}_l^{j+1} - \mathbf{r}_l^j)^2. \quad (15)$$

Here $\mathbf{r}_l^{P+1} = \mathbf{r}_{l+1}^1$, except for $l = N_\uparrow$ for which $\mathbf{r}_{N_\uparrow}^{P+1} = \mathbf{r}_{N_\uparrow-k+1}^1$. In addition, $\omega_P = \sqrt{P}/\beta\hbar$.

$$W_B^{(N_\downarrow)} = \frac{1}{N_\downarrow} \sum_{k=1}^{N_\downarrow} e^{-\beta E_{N_\downarrow}^{(k)}} W_B^{(N_\downarrow-k)}. \quad (16)$$

$$E_{N_\downarrow}^{(k)} = \frac{1}{2} m \omega_P^2 \sum_{l=N_\downarrow-k+1}^{N_\downarrow} \sum_{j=1}^P \left(\mathbf{r}_{N_\uparrow+l}^{j+1} - \mathbf{r}_{N_\uparrow+l}^j \right)^2. \quad (17)$$

Here $\mathbf{r}_{N_\uparrow+l}^{P+1} = \mathbf{r}_{N_\uparrow+l+1}^1$, except for $l = N_\downarrow$ for which $\mathbf{r}_{N_\uparrow}^{P+1} = \mathbf{r}_{N_\uparrow-k+1}^1$.

The expression of $W_B^{(N_\uparrow)}$ ($W_B^{(N_\downarrow)}$) includes the exchange effect by describing all the possible ring polymer configurations for N particles in the internal state $|\uparrow\rangle$ ($|\downarrow\rangle$). The recursion formula for $W_B^{(N_\uparrow)}$ and $W_B^{(N_\downarrow)}$ is the same as that given in Ref.²⁹ for bosons without considering internal state. We see that the evaluation of the partition function still takes $O(PN^3)$ time, rather than $O(PN_\uparrow^3 N_\downarrow^3)$. For two-component spinor bosons there are in total $N_\uparrow! N_\downarrow!$ terms in the partition function summation for different configurations. However, because spin degree of freedom doesn't change, the spin up contribution and spin down contribution to the partition function are unrelated, and the partition function can be divided into two parts and evaluated separately, so the evaluation of the partition function presented in this work takes $O(PN_\uparrow^3 + PN_\downarrow^3)$ times, which is still $O(PN^3)$. However, if the spin degree of freedom has its own dynamics due to spin-changing interaction, then there is no such shortcut and the evaluation of the full partition function now takes $O(PN_\uparrow^3 N_\downarrow^3)$ times.

After we get the final expression of Z_B , we may use massive Nosé-Hoover chain⁴¹⁻⁴⁵ to establish constant temperature for the system, where each degree of freedom of the system has been coupled to a separate Nosé-Hoover thermostat. From the distribution generated by this method, we can calculate the density distribution and energy of the system. For example, the average density is simply given by

$$\rho_\uparrow(\mathbf{x}) = \left\langle \frac{1}{P} \sum_{j=1}^P \sum_{k=1}^{N_\uparrow} \delta(\mathbf{r}_k^j - \mathbf{x}) \right\rangle, \rho_\downarrow(\mathbf{x}) = \left\langle \frac{1}{P} \sum_{j=1}^P \sum_{k=N_\uparrow+1}^N \delta(\mathbf{r}_k^j - \mathbf{x}) \right\rangle. \quad (18)$$

The energy estimator can be obtained from the following expression:

$$E(\beta) = -\frac{1}{Z_B} \frac{\partial Z_B}{\partial \beta}. \quad (19)$$

The energy estimator is

$$E(\beta) = \frac{PdN}{2\beta} + \frac{\langle U \rangle}{P} + \left\langle V_B^{(N_\uparrow)} + \beta \frac{\partial V_B^{(N_\uparrow)}}{\partial \beta} \right\rangle + \left\langle V_B^{(N_\downarrow)} + \beta \frac{\partial V_B^{(N_\downarrow)}}{\partial \beta} \right\rangle. \quad (20)$$

where $V_B^{(N_\uparrow)} = -\frac{1}{\beta} \log W_B^{(N_\uparrow)}$ and $V_B^{(N_\downarrow)} = -\frac{1}{\beta} \log W_B^{(N_\downarrow)}$. $V_B^{(N_\uparrow)} + \beta \frac{\partial V_B^{(N_\uparrow)}}{\partial \beta}$ may be evaluated as

$$V_B^{(N_\uparrow)} + \beta \frac{\partial V_B^{(N_\uparrow)}}{\partial \beta} = \frac{\sum_{k=1}^{N_\uparrow} \left[V_B^{(N_\uparrow-k)} + \beta \frac{\partial V_B^{(N_\uparrow-k)}}{\partial \beta} - E_{N_\uparrow}^{(k)} \right] e^{-\beta(E_{N_\uparrow}^{(k)} + V_B^{(N_\uparrow-k)})}}{\sum_{k=1}^{N_\uparrow} e^{-\beta(E_{N_\uparrow}^{(k)} + V_B^{(N_\uparrow-k)})}}, \quad (21)$$

with $V_B^{(0)} + \beta \frac{\partial V_B^{(0)}}{\partial \beta} = 0$. Similar formulas hold for $V_B^{(N_\downarrow)} + \beta \frac{\partial V_B^{(N_\downarrow)}}{\partial \beta}$. The interaction potential U is given by

$$U = \sum_{j=1}^P V(\mathbf{r}_1^j, \dots, \mathbf{r}_N^j). \quad (22)$$

One may refer to our open-source code with C++ to see the details of the implementation for the simulation of the partition function, energy estimator and density estimator, etc..

III. RESULTS FOR TWO-COMPONENT SPINOR BOSONS

In our PIMD simulation, the number of beads used decreases as temperature increases to ensure numerical stability and assure convergence. Compared with two dimensions with $P = 12/T$ beads in the usual case^{30,32,34}, it is worthy to point out that many more beads are needed to assure accuracy and convergence, because the size of phase space has been greatly enlarged compared with two dimensional case. Based on the relation $\Delta\beta = \beta/P$ and the fact that the evolution operator has been expanded to an order of $O(\Delta\beta^2)$, we would like to keep $\Delta\beta$ a constant with different β , which leads to the choice $P=70/T$. In general, of course, the convergence with respect to the number of beads has to be explicitly verified by increasing the number of beads and check if the results remain the same. It's true that in this way one finds that non-interacting case requires less beads than the interacting case, but we choose the same number of beads for all cases while ensuring that the results converge with respect to the number of beads. Moreover, we performed 12 independent simulations each with at least 10^6 MD steps to establish thermal equilibrium and calculate expectation values. In all of the following we checked convergence with respect to the number of beads and MD steps performed, by increasing P and MD steps and check if we obtain the same results. In our simulation, the statistical fluctuations are negligible. Hence, there is no error bar in all figures for numerical results.

A. Noninteracting spinor Bose gas in 3D harmonic trap

To test our algorithm, we first consider noninteracting identical bosons for $N_{\uparrow} = N_{\downarrow} = 7$ in a three-dimensional harmonic trap with angular frequency ω . We use the natural units of $\hbar = 1, m = 1$ and consider $\omega = 1$. The dimensionless Hamiltonian operator is

$$\hat{H} = \frac{1}{2} \sum_{j=1}^N \hat{\mathbf{p}}_j^2 + \frac{1}{2} \sum_{j=1}^N \hat{\mathbf{r}}_j^2. \quad (23)$$

In Fig. 2(a), the orange circle gives the average energy in our numerical simulation for different temperatures, while the blue circle gives the average energy in grand canonical ensemble for ideal bosons. In this work, the heat capacity is calculated by the finite-difference derivative for the energy with respect to the temperature. In Fig. 2(b), we give the heat capacity $C(T)$ based on the average energy calculated by PIMD. Our simulation shows the presence of a bump in the heat capacity. In the thermodynamic limit, the critical temperature^{46,47} is determined by $k_B T_c = 0.94 \hbar (\omega_x \omega_y \omega_z)^{1/3} N_{\uparrow}^{1/3}$. We have $T_c \approx 1.8$ with our parameters. The peak in our simulation for the heat capacity is at $T_c \approx 1.53$, which is smaller than the result with the formula of the thermodynamic limit. This comparison agrees qualitatively with the result that the finite-size effect has the effect of decreasing the critical temperature^{48,49}.

In Fig. 3, for $k_B T = 0.3$ (in unit of $\hbar \omega$) we give the numerical result of the normalized density distribution $\rho_{\uparrow}(x)$ along x direction by solid circle, while the solid line gives the analytical result of the ground state. For $k_B T \ll \hbar \omega$, the density distribution has the following normalized analytical approximation:

$$\rho_{\uparrow}(x) \simeq \left(\frac{m\omega}{\pi\hbar} \right)^{1/2} e^{-\frac{m\omega}{\hbar} x^2}. \quad (24)$$

Good agreement is found with our simulation results.

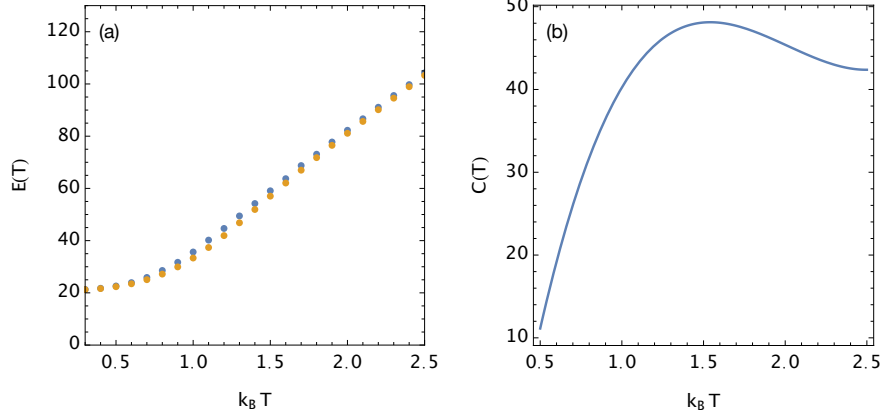


FIG. 2. For $N_{\uparrow} = N_{\downarrow} = 7$ non-interacting bosons in three-dimensional harmonic trap, (a) shows the average energy by PIMD for spinor bosons (orange circle) and the average energy calculated by grand canonical ensemble (blue circle). The good agreement proves the validity and accuracy of our PIMD simulation. (b) shows the heat capacity calculated from the average energy of PIMD, which shows a clear bump as the temperature decreases. The statistical fluctuations are negligible.

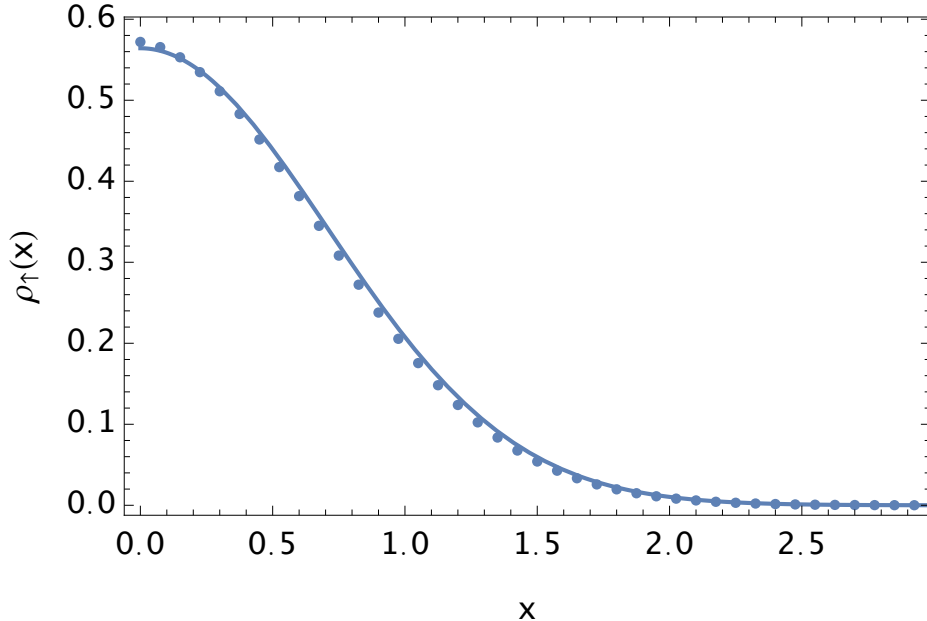


FIG. 3. For $N_{\uparrow} = N_{\downarrow} = 7$ non-interacting bosons in a three-dimensional harmonic trap at the temperature $k_B T = 0.3$, the circle shows the density distribution $\rho_{\uparrow}(x)$ by PIMD, while the solid line is the analytical result of the ground state density distribution. The statistical fluctuations are negligible.

B. Spinor Bose gas in three-dimensional harmonic trap with repulsive Gaussian interaction

The great merit of PIMD for identical bosons lies in that the inclusion of inter-particle interaction will not add too much additional difficulty and calculation error.

We consider the following Gaussian interaction⁵⁰ between bosons

$$V(\mathbf{r}_1, \dots, \mathbf{r}_N) = \frac{1}{2} \sum_{j \neq j'=1}^N \frac{g}{\gamma^2 \pi} e^{-|\mathbf{r}_j - \mathbf{r}_{j'}|^2 / \gamma^2}. \quad (25)$$

We consider here $\gamma = 1$. With length unit $\sqrt{\hbar/m\omega}$ and energy unit $\hbar\omega$, we consider the average energy for $N_{\uparrow} = N_{\downarrow} = 7$ with different coupling constant g . In Fig. 4(a), we show the average energy for different g , while in Fig. 4(b) the heat capacity for different g is given. As expected, at the same temperature, the repulsive interaction has the effect of increasing the total energy. Significant role of the inter-particle repulsive interaction is

shown by the heat capacity, which is still quite challenging to reveal in mean-field theory or the theory beyond the mean-field theory. Our accurate simulations show that the repulsive inter-particle interaction will gradually erase the bump in the heat capacity of ideal bosons. This unique result will provide the benchmark for other methods in future to calculate accurately the thermodynamics of interacting bosons. The disappearance of the bump in the heat capacity is due to the strong interaction between particles.

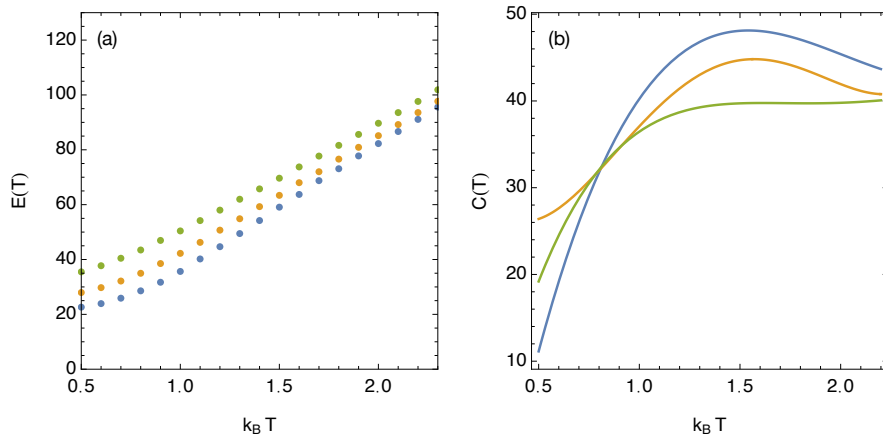


FIG. 4. For $N_{\uparrow} = N_{\downarrow} = 7$ bosons in a three-dimensional harmonic trap with $g = 0$ (blue), $g = 1$ (orange) and $g = 3$ (green), (a) shows the average energy for different g , while (b) shows the heat capacity for different g . As the inter-particle coupling constant increases, we see a gradual disappearance of the bump in the heat capacity. The statistical fluctuations are negligible.

We consider here Gaussian interaction, because for single-component bosons with Gaussian interaction in two dimensions, an analytical expression is given by Mujal et al.⁵⁰ for $N \leq 4$ bosons. Our simulation may give the benchmark for other method to calculate accurately the energy of spinor bosons in three dimensions in future. The s-wave scattering length a may estimated with $\int d^3\mathbf{r} \frac{g}{\gamma^2\pi} e^{-|\mathbf{r}|^2/\gamma^2} = 4\pi\hbar^2 a/m^{47}$. In this case, we have the s-wave scattering length $a = \frac{g\gamma}{4\sqrt{\pi}}$. It is worth pointing out that, to compare with experiments of cold bosonic atoms with s-wave scattering length a , the Gaussian interaction should be chosen to satisfy $a/\bar{l} \ll 1$, with \bar{l} the average interparticle distance.

In Fig. 5, we give the simulation result of the average energy for $N_{\uparrow} = N_{\downarrow} = 3, 4, 5$ with the coupling constant $g = 3$.

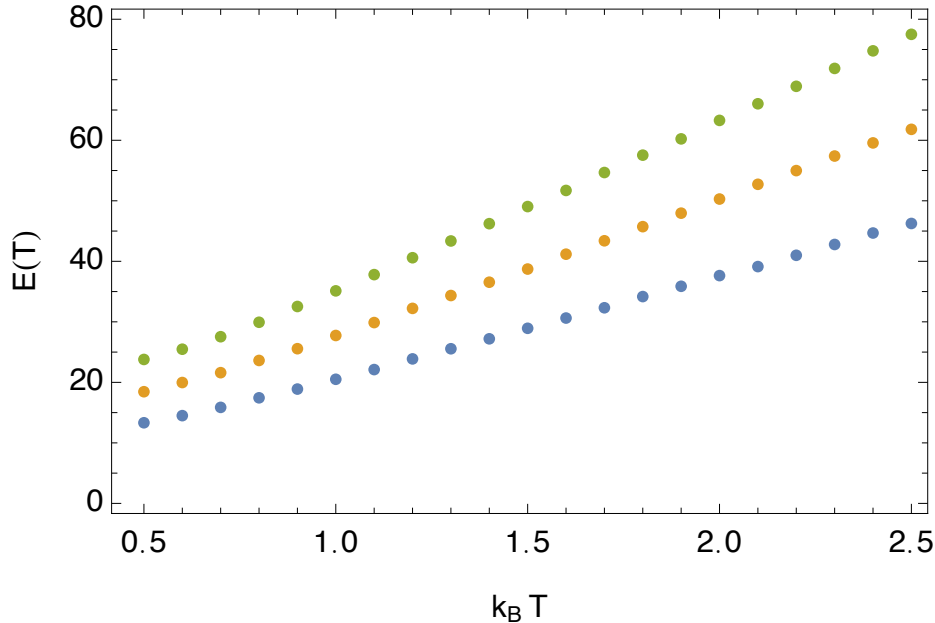


FIG. 5. The simulated energy for $N_\uparrow = N_\downarrow = 3$ (blue), 4 (orange), 5 (green) with the coupling constant $g = 3$. The statistical fluctuations are negligible.

C. Spinor Bose gas in three-dimensional harmonic trap with dipole interaction

Now we consider dipole interaction which is the real situation of spinor Bose gases³⁶. We consider the following simplest dipole interaction

$$V(\mathbf{r}_1, \dots, \mathbf{r}_N) = \frac{1}{2} \sum_{j \neq j'=1}^N \frac{\lambda}{|\mathbf{r}_j - \mathbf{r}_{j'}|^3}. \quad (26)$$

Usually, the realistic dipole interaction comprises of an anisotropic term⁵². The above dipole interaction is also used in path integral Monte Carlo simulations of fermions⁵¹. We use this dipole interaction so that it has the chance to provide the benchmark for other relevant studies.

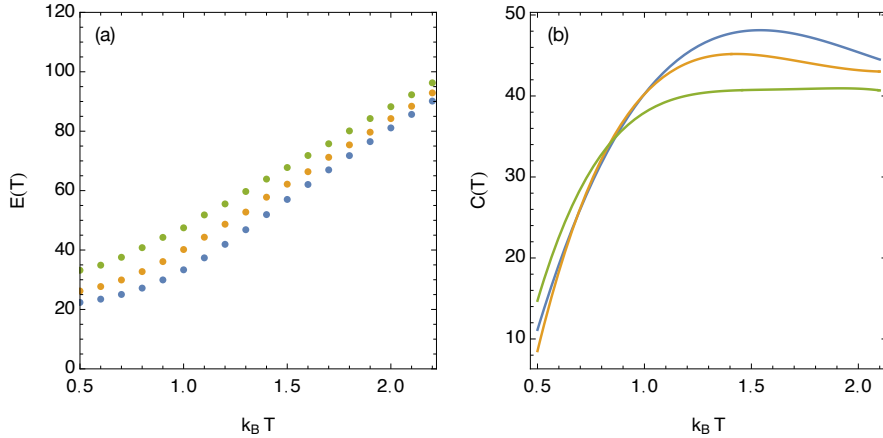


FIG. 6. For $N_\uparrow = N_\downarrow = 7$ bosons in a three-dimensional harmonic trap with dipole interaction, we show the result of different coupling constant $\lambda = 0$ (blue), $\lambda = 0.02$ (orange) and $\lambda = 0.1$ (green). (a) shows the average energy for different λ , while (b) shows the heat capacity for different λ . As the inter-particle coupling constant increases, we see a gradual disappearance of the bump in the heat capacity, which is similar to the case of Gaussian interaction. The statistical fluctuations are negligible.

By varying the interaction strength λ we observed similar phenomenon as we did with Gaussian interaction, as shown in Fig. 6.

IV. GREEN'S FUNCTION AND MOMENTUM DISTRIBUTION

Now we turn to consider the momentum distribution of spinor bosons. In our previous work, we calculated the momentum distribution for single-component bosons in PIMD by first considering Green's function of the system. Our method can be generalized directly to the case of spinor bosons.

For spinor bosons, the thermal Green's function is defined as

$$G_{\uparrow\uparrow}(\mathbf{x}, \tau_1; \mathbf{y}, \tau_2) = \langle \mathcal{T} \{ \hat{\psi}_\uparrow(\mathbf{y}, \tau_2) \hat{\psi}_\uparrow^\dagger(\mathbf{x}, \tau_1) \} \rangle, \quad (27)$$

where $\langle \dots \rangle$ denotes thermal average, \mathcal{T} is the imaginary time-ordering operator. In addition,

$$\hat{\psi}_\uparrow(\mathbf{x}, \tau) = e^{\hat{H}\tau} \hat{\psi}_\uparrow(\mathbf{x}) e^{-\hat{H}\tau}, \quad \hat{\psi}_\uparrow^\dagger(\mathbf{x}, \tau) = e^{\hat{H}\tau} \hat{\psi}_\uparrow^\dagger(\mathbf{x}) e^{-\hat{H}\tau}. \quad (28)$$

Of course, we have $G_{\uparrow\downarrow} = 0$ and $G_{\downarrow\uparrow} = 0$.

To get momentum distribution, we should calculate

$$G_{\uparrow\uparrow}(\mathbf{x}, \tau_2 + \Delta\beta; \mathbf{y}, \tau_2) = \langle \hat{\psi}_{\uparrow}^{\dagger}(\mathbf{x}, \tau_2 + \Delta\beta) \hat{\psi}_{\uparrow}(\mathbf{y}, \tau_2) \rangle. \quad (29)$$

In Fig. 7, we show the idea to calculate this Green's function. One may find the details to implement the algorithm in our previous work. Green's function can be estimated as

$$G_{\uparrow\uparrow}(\mathbf{x}', \tau_1; \mathbf{y}', \tau_2) = \langle \delta(\mathbf{x} - \mathbf{x}') \delta(\mathbf{y} - \mathbf{y}') \rangle, \quad (30)$$

where \mathbf{x} and \mathbf{y} denote the positions of two beads at the end of the gap in Fig. 7.

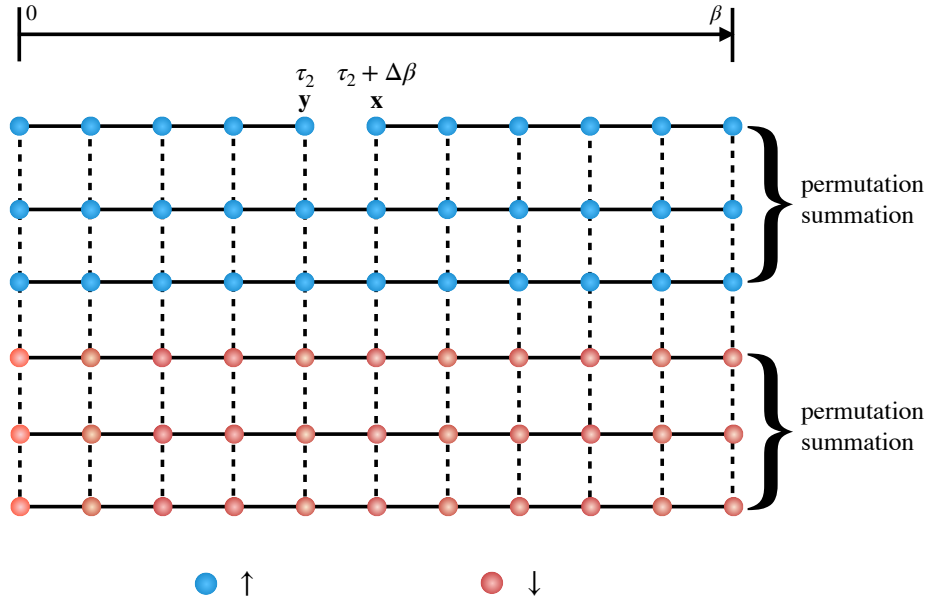


FIG. 7. Modified ring polymers for Green's function $G_{\uparrow\uparrow}$. There is a gap between two beads, from τ_2 to $\tau_2 + \Delta\beta$. In particular, the coordinates of the beads at the ends of the gap are \mathbf{y} and \mathbf{x} . There is no harmonic spring between those two beads.

As illustrated in Fig. 7, there would be a gap for the beads in the top row, due to the field operator $\hat{\psi}_{\uparrow}^{\dagger}(\mathbf{x}, \tau_2 + \Delta\beta) \hat{\psi}_{\uparrow}(\mathbf{y}, \tau_2)$. Following the method given in Ref.³⁰, it is straightforward to write the recursion formula for this Green's function.

Based on thermal Green's function, the momentum distribution is

$$\rho_{\uparrow}(\mathbf{p}) = \frac{1}{(2\pi\hbar)^d} \int d\mathbf{x} d\mathbf{y} G_{\uparrow\uparrow}(\mathbf{x}, \tau_2 + \Delta\beta; \mathbf{y}, \tau_2) e^{\frac{i}{\hbar} \mathbf{p} \cdot (\mathbf{x} - \mathbf{y})}. \quad (31)$$

It is similar to consider $G_{\downarrow\downarrow}(\mathbf{x}, \tau_2 + \Delta\beta; \mathbf{y}, \tau_2)$ and $\rho_{\downarrow}(\mathbf{p})$.

As an application of our method, we consider $N_{\uparrow} = N_{\downarrow} = 8$ bosons in 3D harmonic trap with different dipole interaction at $k_B T = 0.3$. In Fig. 8, we show the momentum distribution along x direction for different λ . We see that as λ increases, the momentum distribution becomes narrower, as expected from the physical picture that repulsive interactions have the effect of increasing the width of the quantum system. At the same temperature, this effect of inter-particle interaction for momentum distribution may be also interpreted by considering Green's function in real space. The ground state wave function is a Gaussian function for non-interacting case, while in the Thoms-Fermi approximation the quadratic behavior is dominating as interaction increases so that it becomes flatter⁴⁷. In experiments, one may use optical lattices⁵³ so that in a lattice site there exists a few or a dozen spinor bosons. By using magnetic-field Feshbach resonance⁵⁴ to turn the inter-particle interaction, we have the chance to show experimentally the behavior of the heat capacity simulated in this work.

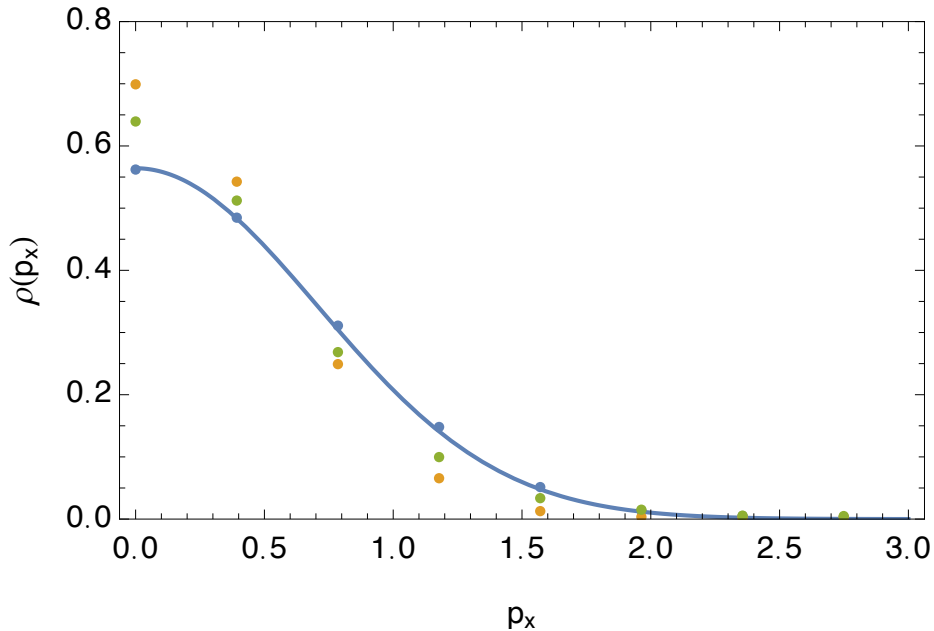


FIG. 8. Shown is the momentum distribution $\rho(p_x)$ of $N_{\uparrow} = N_{\downarrow} = 8$ bosons in 3D harmonic trap with different dipole interaction at $k_B T = 0.3$. The blue circle is the momentum distribution of $\lambda = 0$, while the green circle and orange circle are for $\lambda = 0.5$ and $\lambda = 1$, respectively. The solid line is the momentum distribution of the ground state wave function, which agrees well with our simulation at low temperature. The statistical fluctuations are negligible.

V. CONCLUSION AND DISCUSSION

As a summary, in this work we showed how to generalize the original PIMD methodology to consider spinor bosons and extract thermal properties from our simulations, such as density, heat capacity and momentum distribution. By using our exact numerical method, we are able to study the behavior of heat capacity and we observed that as inter-particle interaction strength increases, the bump in heat capacity curve is gradually erased. Issues worth considering in the future are the compressibility in a harmonic trap, which has been calculated by path integral Monte Carlo for a homogeneous dilute Bose gas and a discontinuous behavior is found at the critical point⁵⁵. We also suggest possible experiment scheme to observe this behavior experimentally. Of course, the method we developed here can be generalized straightforwardly to consider bosons with multiple components and other systems, providing opportunities for future research.

ACKNOWLEDGMENTS

This work is partly supported by the National Natural Science Foundation of China under grant numbers 11175246, and 11334001.

DATA AVAILABILITY

The data that support the findings of this study are available from the corresponding author upon reasonable request. The code of this study is openly available in GitHub (<https://github.com/xiongyunuo/PIMD-Pro-SB-MT>).

REFERENCES

- ¹M. Rossi, L. Salasnich, F. Ancilotto, and F. Toigo, Monte Carlo simulations of the unitary Bose gas, *Phys. Rev. A* **89**, 041602(R) (2014).
- ²L. Parisi, G. E. Astrakharchik, and S. Giorgini, The liquid state of one-dimensional Bose mixtures: a quantum Monte-Carlo study, *Phys. Rev. Lett.* **122**, 105302 (2019).
- ³L. Parisi and S. Giorgini, Quantum droplets in one-dimensional Bose mixtures: a quantum Monte-Carlo study, *Phys. Rev. A* **102**, 023318 (2020).
- ⁴R. P. Feynman and A. R. Hibbs, *Quantum mechanics and path integrals*, Dover Publications, New York (2010).

- ⁵H. Kleinert, Path integrals in quantum mechanics, statistics, polymer physics, and financial markets, World Scientific, Singapore (2009).
- ⁶M. E. Tuckerman, Statistical mechanics: theory and molecular simulation, Oxford University, New York (2010).
- ⁷D. Chandler and P. G. Wolynes, Exploiting the isomorphism between quantum theory and classical statistical mechanics of polyatomic fluids, *J. Chem. Phys.* **74**, 4078 (1981).
- ⁸M. Parrinello and A. Rahman, Study of an F center in molten KCl, *J. Chem. Phys.* **80**, 860 (1984).
- ⁹S. Miura and S. Okazaki, Path integral molecular dynamics for Bose-Einstein and Fermi-Dirac statistics. *J. Chem. Phys.* **112**, 10116 (2000).
- ¹⁰J. Cao and G. A. Voth, The formulation of quantum statistical mechanics based on the Feynman path centroid density. I. Equilibrium properties, *J. Chem. Phys.* **100**, 5093 (1994).
- ¹¹J. Cao and G. A. Voth, The formulation of quantum statistical mechanics based on the Feynman path centroid density. II. Dynamical properties, *J. Chem. Phys.* **100**, 5106 (1994).
- ¹²S. Jang and G. A. Voth, A derivation of centroid molecular dynamics and other approximate time evolution methods for path integral centroid variables, *J. Chem. Phys.* **111**, 2371 (1999).
- ¹³R. Ramírez and T. López-Ciudad, The Schrödinger formulation of the Feynman path centroid density, *J. Chem. Phys.* **111**, 3339 (1999).
- ¹⁴K. Kinugawa, H. Nagao, and K. Ohta, Path integral centroid molecular dynamics method for Bose and Fermi statistics: formalism and simulation, *Chem. Phys. Lett.* **307**, 187 (1999).
- ¹⁵Pierre-Nicholas Roy, Seogjoo Jang, and Gregory A. Voth, Feynman path centroid dynamics for Fermi-Dirac statistics, *J. Chem. Phys.* **111**, 5303 (1999).
- ¹⁶P.-N. Roy and G.A. Voth, On the Feynman path centroid density for Bose-Einstein and Fermi-Dirac statistics, *J. Chem. Phys.* **110**, 3647 (1999).
- ¹⁷N. Blinov, P.-N. Roy, and G.A. Voth, Path integral formulation of centroid dynamics for systems obeying Bose-Einstein statistics, *J. Chem. Phys.* **115**, 4484 (2001).
- ¹⁸N. Blinov and P.-N. Roy, Operator formulation of centroid dynamics for Bose-Einstein and Fermi-Dirac statistics, *J. Chem. Phys.* **115**, 7822 (2001).

- ¹⁹K. Kinugawa, A semiclassical approach to the dynamics of many-body Bose/Fermi systems by the path integral centroid molecular dynamics, *J. Chem. Phys.* **114**, 1454 (2001).
- ²⁰K. Kinugawa, H. Nagao, and K. Ohta, A path integral centroid molecular dynamics method for Bose and Fermi statistics, *J. Mol. Liq.* **90**, 11 (2001).
- ²¹Nicholas Blinov and Pierre-Nicholas Roy, An effective centroid Hamiltonian and its associated centroid dynamics for indistinguishable particles in a harmonic trap, *J. Chem. Phys.* **116**, 4808 (2002).
- ²²Pierre-Nicholas Roy and Nicholas Blinov, Centroid dynamics with quantum statistics, *Isr J. Chem.* **42**, 183 (2002).
- ²³Paul Moffatt, Nicholas Blinov, and Pierre-Nicholas Roy, On the calculation of single-particle time correlation functions from Bose–Einstein centroid dynamics, *J. Chem. Phys.* **120**, 4614 (2004).
- ²⁴E. A. Polyakov, A. P. Lyubartsev, and P. N. Vorontsov-Velyaminov, Centroid molecular dynamics: Comparison with exact results for model systems, *J. Chem. Phys.* **133**, 194103 (2010).
- ²⁵I. R. Craig and D. E. Manolopoulos, Quantum statistics and classical mechanics: Real time correlation functions from ring polymer molecular dynamics, *J. Chem. Phys.* **121**, 3368 (2004).
- ²⁶B. J. Braams and D. E. Manolopoulos, On the short-time limit of ring polymer molecular dynamics, *J. Chem. Phys.* **125**, 124105 (2006).
- ²⁷S. Habershon, D. E. Manolopoulos, T. E. Markland, and T. F. Miller 3rd, Ring-polymer molecular dynamics: quantum effects in chemical dynamics from classical trajectories in an extended phase space, *Annu. Rev. Phys. Chem.* **64**, 387 (2013).
- ²⁸T. E. Markland and M. Ceriotti, Nuclear quantum effects enter the mainstream, *Nat. Rev. Chem.* **2**, 0109 (2018).
- ²⁹B. Hirshberg, V. Rizzi, and M. Parrinello, Path integral molecular dynamics for bosons, *Proc. Natl. Acad. Sci. U. S. A.* **116**, 21445 (2019).
- ³⁰Y. N. Xiong and H. W. Xiong, Path integral molecular dynamics simulations for Green’s function in a system of identical bosons, *J. Chem. Phys.* **156**, 134112 (2022).
- ³¹C. W. Myung, B. Hirshberg, and M. Parrinello, Prediction of a supersolid phase in high-pressure deuterium, *Phys. Rev. Lett.* **128**, 045301 (2022).
- ³²Y. N. Xiong and H. W. Xiong, Path integral and winding number in singular magnetic

- field, *Eur. Phys. J. Plus* **137** 550 (2022).
- ³³B. Hirshberg, M. Invernizzi, and M. Parrinello, Path integral molecular dynamics for fermions: Alleviating the sign problem with the Bogoliubov inequality, *J. Chem. Phys.* **152**, 171102 (2020).
- ³⁴Y. N. Xiong and H. W. Xiong, Numerical calculation of Green's function and momentum distribution for spin-polarized fermions by path integral molecular dynamics, *J. Chem. Phys.* **156**, 204117 (2022).
- ³⁵Y. N. Xiong and H. W. Xiong, A solution of fermion sign problem for large fermion systems, *arXiv:2206.08341* (2022).
- ³⁶Yuki Kawaguchia and Masahito Ueda, Spinor Bose–Einstein condensates, *Physics Reports* **520**, 253 (2012).
- ³⁷H. -J. Miesner, D. M. Stamper-Kurn, J. Stenger, S. Inouye, A. P. Chikkatur, and W. Ketterle, Observation of Metastable States in Spinor Bose-Einstein Condensates, *Phys. Rev. Lett.* **82**, 2228 (1999).
- ³⁸L. Sadler, J. Higbie, S. Leslie, M. Vengalattore, and D. M. Stamper-Kurn, Spontaneous symmetry breaking in a quenched ferromagnetic spinor Bose–Einstein condensate, *Nature* **443**, 312 (2006).
- ³⁹Li Chen, Han Pu, and Yunbo Zhang, Spin-orbit angular momentum coupling in a spin-1 Bose-Einstein condensate, *Phys. Rev. A* **93**, 013629 (2016).
- ⁴⁰Chunji Wang, Chao Gao, Chao-Ming Jian, and Hui Zhai, Spin-Orbit Coupled Spinor Bose-Einstein Condensates, *Phys. Rev. Lett.* **105**, 160403 (2010).
- ⁴¹S. Nosé, A molecular dynamics method for simulations in the canonical ensemble, *Mol. Phys.* **52**, 255 (1984).
- ⁴²S. Nosé, A unified formulation of the constant temperature molecular dynamics methods, *J. Chem. Phys.* **81**, 511 (1984).
- ⁴³W. G. Hoover, Canonical dynamics: Equilibrium phase-space distributions, *Phys. Rev. A* **31**, 1695 (1985).
- ⁴⁴G. J. Martyna, M. L. Klein, and M. Tuckerman, Nosé-Hoover chains: The canonical ensemble via continuous dynamics, *J. Chem. Phys.* **97**, 2635 (1992).
- ⁴⁵S. Jang and G. A. Voth, Simple reversible molecular dynamics algorithms for Nosé-Hoover chain dynamics, *J. Chem. Phys.* **107**, 9514 (1997).
- ⁴⁶V. Bagnato, David E. Pritchard, and D. Kleppner, Bose-Einstein condensation in an ex-

- ternal potential, *Phys. Rev. A* **35**, 4354 (1987).
- ⁴⁷Lev. P. Pitaevskii and S. Stringari, *Bose Einstein condensation and superfluidity*, Oxford University Press, New York (2016).
- ⁴⁸S. Liu, G. Huang, L. Ma, S. Zhu, and H. Xiong, Thermodynamic properties of the trapped interacting Bose gas with finite size, *J. Phys. B: At. Mol. Opt. Phys.* **33**, 3911 (2000).
- ⁴⁹H. Xiong, S. Liu, G. Huang, Z. Xu, and C. Zhang, Critical temperature and condensate fraction of the trapped interacting Bose gas with finite-size effects, *J. Phys. B: At. Mol. Opt. Phys.* **34**, 3013 (2001).
- ⁵⁰P. Mujal, E. Sarlé, A. Polls, B. Juliá-Díaz, Quantum correlations and degeneracy of identical bosons in a two-dimensional harmonic trap, *Phys. Rev. A* **96**, 043614 (2017).
- ⁵¹T. Dornheim, Fermion sign problem in path integral Monte Carlo simulations: Quantum dots, ultracold atoms, and warm dense matter, *Phys. Rev. E* **100**, 023307 (2019).
- ⁵²J. Stuhler, A. Griesmaier, T. Koch, M. Fattori, T. Pfau, S. Giovanazzi, P. Pedri, and L. Santos, Observation of Dipole-Dipole Interaction in a Degenerate Quantum Gas, *Phys. Rev. Lett.* **95**, 150406 (2005).
- ⁵³M. Greiner, O. Mandel, T. Esslinger, Theodor W. Hänsch, and I. Bloch, *Nature* **415**, 39 (2002).
- ⁵⁴C. Chin, R. Grimm, P. Julienne, and E. Tiesinga, *Rev. Mod. Phys.* **82**, 1225 (2010).
- ⁵⁵G. Spada, S. Pilati, and S. Giorgini, Thermodynamics of a dilute Bose gas: A path-integral Monte Carlo study, *Phys. Rev. A* **105**, 013325 (2022).